



Cite this: *Soft Matter*, 2020, 16, 7751

Packing and dynamics of a protein solution approaching the jammed state†

Nafisa Begam,^{ib}*^a Stefano Da Vela,^{ib}‡^a Olga Matsarskaia,^{ib}§^a Michal K. Braun,^a Alessandro Mariani,^{ib}¶^b Fajun Zhang^{ib}*^a and Frank Schreiber^{ib}^a

The packing of proteins and their collective behavior in crowded media is crucial for the understanding of biological processes. Here we study the structural and dynamical evolution of solutions of the globular protein bovine serum albumin with increasing concentration *via* drying using small angle X-ray scattering and dynamic light scattering. We probe an evolving correlation peak on the scattering profile, corresponding to the inter-protein distance, ζ , which decreases following a power law of the protein volume fraction, ϕ . The rate of decrease in ζ becomes faster above a protein concentration of $\sim 200 \text{ mg ml}^{-1}$ ($\phi = 0.15$). The power law exponent changes from 0.33, which is typical of colloidal or protein solutions, to 0.41. During the entire drying process, we observe the development and the growth of two-step relaxation dynamics with increasing ϕ as revealed by dynamic light scattering. We find three different regimes of the dependence of ζ as a function of ϕ . In the dilute regime ($\phi < 0.22$), protein molecules are far apart from each other compared to their size. In this case, the dynamics mainly corresponds to Brownian motion. At an intermediate concentration ($0.22 < \phi < 0.47$), inter-protein distances become comparable to the size of protein molecules, leading to a preferential orientation of the ellipsoidal protein molecules along with a possible deformation. In this regime, the dynamics shows two distinct relaxation times. At a very high concentration ($\phi > 0.47$), the system reaches a jammed state. Subsequently, the secondary relaxation time in this state becomes extremely slow. In this state, the protein molecules have approximately one hydration layer. This study contributes to the understanding of protein molecular packing in crowded environments and the phenomenon of density-driven jamming for soft matter systems.

Received 23rd May 2020,
Accepted 22nd July 2020

DOI: 10.1039/d0sm00962h

rsc.li/soft-matter-journal

1 Introduction

The properties of concentrated protein solutions have a substantial impact on the application of biopolymeric materials in pharmaceuticals,^{1–3} preservation of biological materials,^{4,5} and foods.^{6,7} Understanding the structural properties of proteins in a concentrated medium is therefore essential to research areas concerned with human health.⁸ The presence of crowding agents has been shown to influence protein–protein interactions, and the aggregation of proteins.^{9–11} The crowded environment in living cells with a macromolecular volume fraction of up to

40% has a relevant impact on the effective structural conformation of proteins. In such an environment, the typical intermolecular distance can be smaller than the native size of the protein molecules in dilute solutions.¹² In addition to structural changes, experimental results have demonstrated a strong effect of macromolecular crowding on many biological processes.^{8,13,14} Enhancement of reaction rates and a subsequent reduction in excluded volume was attributed to crowding in a review article by Zhou *et al.*¹⁵ A change in the shape of aspherical proteins due to crowding was reported in a study combining experimental results with computational studies by Homouz *et al.*¹² However, a clear understanding of the structural packing of globular proteins in a crowded medium is still to be obtained. In this context, a very important factor is the protein hydration shell,^{16,17} which consists of one or few water layers surrounding the protein molecule that interact with it. It thus plays a major role in determining protein stability and functions. Investigation of the protein hydration shell benefits the interpretation of many biophysical experimental results obtained by techniques such as NMR spectroscopy, X-ray crystallography and neutron diffraction.

^a Institut für Angewandte Physik, Universität Tübingen, 70276, Tübingen, Germany.
E-mail: nafisa.begam@uni-tuebingen.de, fajun.zhang@uni-tuebingen.de

^b ESRF-The European Synchrotron, 71 Avenue des Martyrs, 38000, Grenoble, France

† Electronic supplementary information (ESI) available. See DOI: 10.1039/d0sm00962h

‡ Present address: EMBL c/o DESY, Notkestr. 85, 22607 Hamburg, Germany.

§ Present address: Institut Laue-Langevin, 71 Avenue des Martyrs, 38042 Grenoble, France.

¶ Present address: Helmholtz-Institut Ulm für Elektrochemische Energiespeicherung, Helmholtzstr. 11, 89081 Ulm, Germany.

Apart from structural effects, transport properties of globular proteins in a crowded medium are crucial since protein diffusion has a strong impact on their functions.¹⁸ Therefore, a systematic understanding of the influence of concentration on protein dynamics is essential.^{19,20} Neutron scattering studies revealed a robust reduction in the self-diffusion coefficients as a function of volume fraction of the protein bovine serum albumin (BSA),^{20,21} whereas a dynamic light scattering study on bovine lens homogenate over a large range of concentrations disclosed the influence of crowding on the self- and the collective diffusion coefficients and attributed this effect to the dominating direct inter-protein interaction at high volume fractions.^{22,23} Nevertheless, a connection between structural packing and slow dynamics at volume fractions near a jammed state for a globular protein system is still not well established.

Globular proteins, in principle, can be viewed as being similar to colloidal systems and there have been several approaches to understand their phase behavior in a colloidal picture.^{24–27} In the case of hard spheres, the elastic modulus diverges at a volume fraction of 0.64, leading to a jammed state^{28–30} and the close packed structure is reflected in a strong structure factor peak.³¹ A successful explanation of this phenomenon in the hard sphere model is achieved by mode-coupling theory which suggests that the dynamical arrest of the system occurs due to coupling of different fluctuation modes.³² With an attractive interaction between the particles, this transition to arrest occurs even earlier.^{33,34} However, hard colloids, as opposed to proteins, do not change their shape upon external crowding.^{12,35} Proteins, in contrast, are more similar to soft colloids which can compress, deform and interpenetrate.³⁶ In addition, soft colloids have also been found to reach a jammed state similar to that of hard spheres.^{37–41} Along these lines, the formation of a dynamically arrested state of hard spheres with a soft interaction potential has been successfully applied to concentrated protein solutions.⁴² However, a comprehensive picture of protein packing in a jammed/glassy state is yet to be established.

This topic inspired us to investigate the structural and dynamical evolution of aqueous protein solutions while approaching the “critical” volume fraction near the jammed state and to understand the influence of protein softness on this process. In this report, we study the structural and the dynamical evolution of BSA in aqueous solution, without additives, during evaporation of the solvent leading to a gradual increase in BSA concentration. BSA is a globular protein with a shape which can be roughly described by an ellipsoid.²¹ The dry BSA dimensions are $1.25 \times 4.19 \times 4.19 \text{ nm}^3$ (ref. 43). However, in spite of its non-spherical shape, BSA has been often described successfully as a spherical particle with a radius of 3.3–3.7 nm and has a volume of 88–92 nm³ (ref. 44–47). Likely due to the self-buffering of BSA molecules^{48,49} in solution, the pH of the solution remains at *ca.* 6.8 over a large concentration range. In the current study, throughout solvent evaporation, the system preserves a homogeneous, transparent appearance. A monotonic decrease of the correlation length scale (inter-protein distance) is observed. Upon further increase of volume

fraction, the decrease of the correlation length scale slows down. The system eventually reaches a jammed state beyond a “critical” volume fraction, ϕ_c . Our results indicate two-step relaxation dynamics at high volume fractions suggesting caged motion of the protein molecules where the relaxation time follows Vogel–Fulcher–Tammann (VFT) relation as a function of volume fraction.^{50,51}

2 Experimental section

BSA was purchased from Sigma Aldrich (A7906) and was used as received. It was dissolved in de-gassed de-ionized water (18 MΩ cm, MilliQ, Merck, Darmstadt) and stored overnight at 4 °C to obtain a homogeneous solution. The concentration of the stock solution was determined by UV-vis absorption at $\lambda = 280 \text{ nm}$ and was equal to 320 mg ml^{-1} .⁵² The extinction coefficient used for the concentration determination was $0.667 \text{ mg}^{-1} \text{ ml cm}^{-1}$ (ref. 52 and 53). A film was made from this solution by dipping a metal ring into the solution. The metal ring is shown in the inset of Fig. 1(b). Small angle X-ray scattering (SAXS) experiments were performed on this film by mounting it on the SAXS sample stage of our home SAXS instrument (Xeuss 2.0, Xenocs, France) as well as on beamline ID02 of the ESRF (Grenoble, France) at room temperature. In order to calibrate the structure factor peak at different volume fractions of BSA, we prepared a series of solutions over a range of concentrations by diluting the stock solution with de-ionized water. The exact BSA concentration, c_p , of each solution was obtained by UV-vis absorption spectroscopy. For SAXS experiments on ID02, the solutions were filled into quartz capillaries

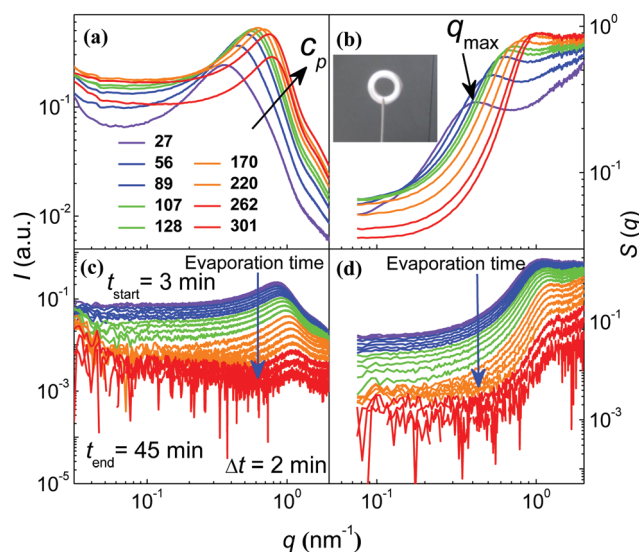


Fig. 1 (a) SAXS profiles of BSA solutions at different concentrations collected at ID02 and (b) corresponding structure factors, $S(q)$ (see ESI,† Fig. S1 and S2). c_p of the solutions are given in the legend in mg ml^{-1} . (c) Time series of SAXS profiles collected during the evaporation of BSA (collected at ID02) and (d) $S(q)$ showing the evolution of the correlation peak with evaporation time (indicated by arrow). The first SAXS profile is collected at time $t_{\text{start}} = 3 \text{ min}$ and successive SAXS profiles are collected at time intervals of $\Delta t = 2 \text{ min}$. Inset shows a photograph of the metal ring used for the SAXS measurements.

with a diameter of 2 mm. The X-ray energy was 12.46 keV, the wavelength, λ was 0.998 Å, the sample to detector distance was 2.3 m, the exposure time was 0.5 s for each measurement, and the scattering wave vector transfer q ($= \frac{4\pi \sin \theta}{\lambda}$, where λ is the wavelength of the incident X-ray beam and 2θ is the scattering angle) range was 0.017–3.8 nm⁻¹. For the experiment on the home SAXS setup, λ was 1.54 Å, the sample to detector distance was 1.6 m, the exposure time was 300 s for each measurement, and the q range was 0.06 to 3.0 nm⁻¹.

Dynamic light scattering (DLS) measurements were performed on the BSA solutions (at room temperature) to investigate the dynamics⁵⁴ using an ALV-CGS3 setup (Germany). The wavelength of the incident light was $\lambda = 632.8$ nm. The solutions were filled into glass cuvettes with a diameter of 10 mm and placed into the sample chamber. DLS probes the intensity auto-correlation function, $g_2(t)$ given by⁵⁵

$$g_2(t) = \frac{\langle I(t_0)I(t_0 + t) \rangle}{\langle I(t_0) \rangle^2} \quad (1)$$

where $I(t_0)$ is the scattered intensity recorded at time t_0 . The characteristic relaxation time τ , probed at the length scale of $2\pi/q$ (where $q = \frac{4\pi n}{\lambda} \sin \theta$, n being the refractive index of the solvent, water in this case) can be determined using the Kohlrausch–Williams–Watts (KWW) equation^{56,57}

$$g_2(t) = 1 + \beta \exp[-2(t/\tau)^\gamma] \quad (2)$$

where γ is the stretching exponent and β is the instrumental factor. In the case of two-component dynamics, the above equation can be expressed as

$$g_2(t) = 1 + \beta \{ A_1 \exp[-2(t/\tau_1)^\gamma] + A_2 \exp[-2(t/\tau_2)^\gamma] \} \quad (3)$$

where the fast and slow components in the dynamics, here tentatively related to individual protein molecules and aggregates, are denoted by 1 and 2, respectively.

The initial concentration of the solution investigated by DLS was $c_p = 317$ mg ml⁻¹. Consecutive DLS experiments were performed on it during the drying process. After each measurement, the solution was kept under a fume hood with laminar flow to allow for solvent evaporation. The total weight of the solution was simultaneously recorded to estimate the amount of water evaporated during this process and thus determine the concentration of the solution at the time of each DLS measurement. In order to avoid the development of any concentration gradient inside the solution, we kept the evaporation rate low (approximately 23 mg per day). However, towards the end of the measurement series (after 35–40 days), a concentration gradient was observed along the wall of the cuvette. At this point, the measurements were terminated.

The volume fraction dependence of the relaxation time was also determined (at low ϕ) by performing DLS measurements on a series of dilute BSA solutions of known concentrations. The data collected on a such series of solutions combined with that collected on the drying sample (presented in Section 4) allow us to obtain $g_2(t)$ over a wide range of ϕ (0.003–0.43).

3 Results and discussion

SAXS intensity profiles as a function of q for different protein concentrations are shown in Fig. 1(a).⁵⁸ The scattering profile collected on a capillary filled with water was used for the background correction for this data set. The structure factors $S(q)$ are shown in Fig. 1(b), where the peak position q_{\max} is related to the characteristic length scale of the solution, $\zeta = 2\pi/q_{\max}$. q_{\max} is found to increase as c_p increases. This implies that ζ , *i.e.* the inter-protein distance, decreases with increasing c_p . This observation is, of course, in line with the results obtained on colloidal systems.^{59,60}

We note that the structure factors might be influenced by the solution pH, ionic strength or the generally non-spherical shape of proteins. Nevertheless, it has been shown that the intensity profile of a system consisting of ellipsoidal particles can be modeled using a system of spherical particles with a finite size distribution⁶¹ for the present purpose. This means that spherical models with a finite size distribution and ellipsoidal models lead to very similar results. In addition, the pH value in the current study was found to stabilize at *ca.* 6.8 for c_p values between 27–301 mg ml⁻¹ (see Fig. S3, ESI†). The pH of the solution is hence not expected to significantly change the effective diameter of the native BSA molecules with changing c_p .⁴⁵

Ideally, one might wish to study ζ near the glass transition of BSA. However, obtaining a protein solution with such a high volume fraction is rather cumbersome.⁴⁵ Therefore, we performed *in situ* SAXS measurements while letting the water evaporate from the solution (“drying” the film on the metal ring) which increases the volume fraction. The evaporation experiment was performed in air at a temperature of 21 °C and at ~40% humidity (conditions at ID02). The intensity profiles during drying of the solution over time are shown in Fig. 1(c). In this case, the scattering profile after complete evaporation of the sample, which is essentially flat, was used for background correction. The SAXS profiles were taken in time intervals of 2 min. $S(q)$ obtained during the drying process represented in Fig. 1(d) shows a gradual shifting of the peak to higher q , indicating a reduction of ζ with time as a result of increasing volume fraction. The peak eventually disappears, suggesting that an essentially homogeneous state is reached. The decrease in overall intensity is possibly due to the gradual reduction in the electron density contrast. In order to quantify the propagation of ζ , we plotted ζ vs. time as well as protein concentration, c_p which is summarized in Fig. 2.

The black circles in Fig. 2 represent the c_p dependence of ζ (obtained from $S(q)$, Fig. 1(b)) as a power law of c_p , initially with an exponent of 0.33 (see ref. 59, 60 and 62). The fit of this part of the data is represented by the red line. At later stages, the slope changes to ~0.41 at $c_p \sim 200$ mg ml⁻¹ and the fit is represented by the green line. Measurements using the laboratory SAXS instrument (Fig. S4, ESI†) also show a similar behavior of ζ in terms of values and the power law of q , which reproduces the results regardless of the experimental conditions. Note that the exponent larger than 1/3 at high

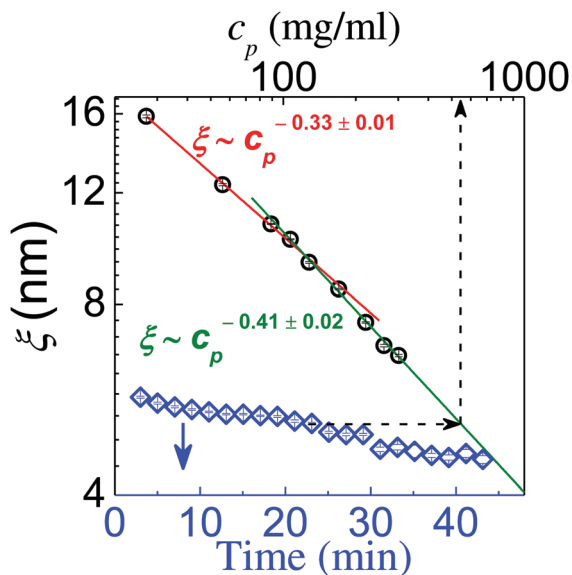


Fig. 2 ξ as a function of c_p (black circles) estimated from independent SAXS measurements performed at different concentrations (top x-axis) of BSA exhibits a power law, $\xi \sim c_p^\alpha$, with $\alpha = 0.33$ (red line) and 0.41 (green line) for c_p below and above 200 mg ml^{-1} , respectively, and ξ (blue diamonds) as a function of drying time (bottom x-axis). The black dashed line illustrates how each ξ relates to its corresponding c_p value. Error bars are smaller than the symbols. Standard deviations of α obtained from the fits are very small and are thus possibly under-estimated.

concentrations is possibly due to the combination of the screening effect of the counterions (released from proteins), the ellipsoidal shape of BSA and its deformation at a high packing density.^{37,63} The power law dependence is better visualized in Fig. S5 (ESI[†]) showing the calibration curve on a linear scale. The length scale varies by more than a factor of 2 in the concentration range of $27\text{--}301 \text{ mg ml}^{-1}$ and two distinct power law behaviors can be observed here. For comparison, we have also modeled the full range of data with a single power law and obtained an exponent of 0.36 (Fig. S6 and S7, ESI[†]). The presence of two distinct power laws in ξ vs. c_p plot could also be observed when extracting the q_{max} from the SAXS intensity profile as shown in Fig. S8 (ESI[†]).

The time dependence of ξ , obtained from $S(q)$ during drying, is represented by the blue diamonds in Fig. 2. It is interesting to observe that, in the beginning of the drying process, ξ , ($= 5.7 \text{ nm}$) is already smaller than the molecular size of a native BSA protein, σ (6.8 nm)⁴⁴ and eventually decreases to a value of 4.6 nm . In the limiting case, if we were to assume a face centred cubic (fcc)-like packing of molecules,⁶⁴ on average, in the beginning of drying, we obtain the lattice constant a as

$$a = \sqrt{2} \times \xi = \sqrt{2} \times 5.7 = 8.1 \text{ nm} \quad (4)$$

This implies a volume per BSA molecule

$$V_{\text{BSA}} = \frac{1}{4} \times 8.1^3 \text{ nm}^3 = 133 \text{ nm}^3 \quad (5)$$

Although at this packing, the inter-particle distance is smaller than the native BSA monomer diameter, the effective volume for each BSA molecule is still higher than the native

volume of 81 nm^3 (calculation shown in the ESI[†])⁶⁵ in dilute solutions. This could be due to a combined effect of alignment of the ellipsoidal BSA molecules in such a way that the inter-protein distance is smaller than the average size of the molecules and also the deformation of the molecules. At the highest volume fraction, the length scale $\xi = 4.6 \text{ nm}$ implies a molecular volume of 69 nm^3 which is smaller than the dry volume (81 nm^3) and is, thus, not possible in the current experimental condition. However, the ξ ($= 5.58 \text{ nm}$) obtained instead from $I(q)$ (see Fig. S8, ESI[†]) implies $V_{\text{BSA}} = 123 \text{ nm}^3$ which is close to some experimental volumes of hydrated BSA. Such a difference in the values of ξ and hence in V_{BSA} could be due to the fact that the determination of q_{max} from $S(q)$ leads to a systematic shift in q_{max} (see Fig. S2, ESI[†]) as the peak intensity is significantly reduced, and the packing is possibly different from fcc at a very high volume fraction (such as in the dried state). As a next step, we aimed at determining the volume fraction at which the regime with $\xi < \sigma$ was observed.

For this purpose, we used the power law which was found from the concentration calibration at higher concentrations. Hence, the c_p corresponding to each ξ during the drying process was estimated from the power law (Fig. 2)

$$\xi \sim c_p^{-0.41 \pm 0.02} \quad (6)$$

From this relation, we estimated the volume fraction (ϕ) of the system using the relation $\phi = c_p \times V_s$, where $V_s = 0.735$ (in $\text{cm}^3 \text{ g}^{-1}$) is the specific volume of BSA^{65,66} (c_p in g ml^{-1}). The evolution of c_p and ϕ as a function of drying time is summarized in Fig. 3(a).

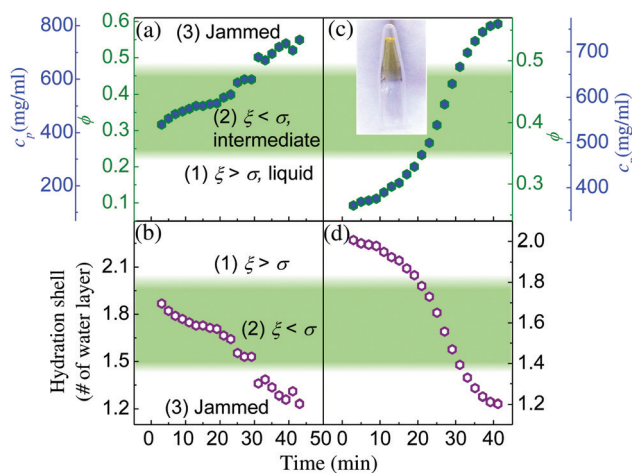


Fig. 3 (a) Volume fraction of the BSA solutions, estimated from a power law dependence of ξ (obtained from $S(q)$) on solution concentrations as a function of drying time revealing three different regimes identified in this work: liquid state at low volume fraction, jammed at high volume fraction and intermediate state (with green background) with possible orientation and deformation of the molecules, (b) number of water layers as a function of drying time. For comparison, volume fractions and number of water layers as a function of drying time estimated from $I(q)$ are shown in (c) and (d), respectively. Inset shows a photograph of the transparent sample after complete solvent evaporation.

The entire evaporation process suggests three distinct regimes (indicated as (1), (2), (3) in Fig. 3(a)). An experimental report⁴⁵ on BSA viscosity measurements with varying volume fraction suggests a glass-like transition with a kinetic arrest at a mass fraction of 0.55, which corresponds to $\phi \approx 0.47$ (calculation shown in ESI†). Beyond a mass fraction of 0.6 ($\phi \approx 0.52$), the material was observed to behave like a solid. Therefore, regime (3) beyond a volume fraction of 0.47 is marked as a jammed state in the current study. It is possible that the water evaporation kinetics (rate of evaporation) influences the shape of the ξ versus time plot. However, the absolute value of ϕ (which is very high) obtained from ξ (using eqn (6)) as well as stopping of the growth of ϕ indicates such solid-like behavior. The lower volume fractions (the calibration regime in the present study) yield a regime where molecules are in their native shape as marked in Fig. 3(a).⁴⁵

Interestingly, there is a crossover point at which ξ becomes smaller than the protein diameter, 6.8 nm (in particular, at the end of the calibration). In Fig. 3(a), this transition (from regime (1) to (2)), as obtained from $S(q)$, is indicated at $\phi \sim 0.22$ (at $c_p \sim 300 \text{ mg ml}^{-1}$, determined from the calibration). We have determined the volume fractions during drying from $I(q)$ as well, which are shown in Fig. 3(c). In this case, the transition is indicated at $\phi \sim 0.35$. A steady decrease in inter-protein distance is observed up to this volume fraction. At this “critical volume fraction”, the system enters the regime with ξ smaller than the molecular size, possibly due to orientation and deformation of the molecules due to the soft inter-protein interactions.⁶⁷ The drop of the scattering intensity to zero in the case of various systems has been considered as the signature of a homogeneous state.^{62,68} In the current study, at a ϕ higher than 0.52 (regime (3)), the peak evolution slows down significantly and the intensity drops to almost zero. This is possibly due to the homogenization as well as solidification of the system at such a high volume fraction. As the volume fraction increases, the deformation and interpenetration of proteins lead to a homogeneous state and the electron density contrast decreases. As a result, the SAXS correlation peak disappears at a certain time. Note that the phase behavior of BSA during drying obtained directly from $I(q)$ is similar to that obtained from $S(q)$ implying that both methods reflect the same behavior.

The inter-particle distance in a colloidal suspension has been proposed (ref. 69 and 70) to follow a slightly different relation, $\xi = \frac{2.25\pi}{q_{\text{max}}}$ (ref. 69 and 70) approaching a jammed state. We recalculated ξ using this relation and show the values thus obtained in the ESI† (Fig. S9). Also in this case, the distance ξ decreases to a length smaller than σ (at $\phi = 0.3$), likewise indicating the potential influence of the non-spherical shape or of the deformation of the molecule. Particles of ellipsoidal shape can pack more densely than spherical ones, and their volume fraction can reach up to 0.68–0.74 (ref. 37, 63 and 71). On the other hand, the deformation of soft particles can lead a system to even much higher volume fraction than its jamming transition.^{37,38,72} In the current study, the molecular packing is possibly influenced by both ellipsoidal shape as well as the deformation which leads to an exponent higher than 1/3 of the power law dependence of ξ on c_p .

We further estimated the hydration level at this stage using experimentally determined dimensions of the bare BSA and the hydrated BSA, approximated as ellipsoids, which are,⁴³

$$V_{\text{bare}}^{(\text{exp})} \sim 1.25 \times 4.19 \times 4.19 \text{ nm}^3 \quad (7)$$

and

$$V_{\text{hydr}}^{(\text{exp})} \sim 1.7 \times 4.2 \times 4.2 \text{ nm}^3. \quad (8)$$

Therefore, the volume fraction of one water layer around one BSA molecule is

$$\phi_{\text{hydr}} = \frac{V_{\text{hydr}}^{(\text{exp})} - V_{\text{bare}}^{(\text{exp})}}{V_{\text{bare}}^{(\text{exp})}} = 36.6\% \quad (9)$$

The water volume fraction ($1 - \phi$) was divided by this value to estimate the number of water layers (Fig. 3(b)). As expected, the number of water layers decreases with drying time. Eventually, approximately 1 water molecule layer per BSA molecule is present at the highest concentration. The decrease of the small-angle scattering intensity to the background level (*i.e.* disappearance of the contrast) at the highest BSA concentration (dried sample) points to a homogeneous state. This could be due to the very low electron density contrast between protein molecules and the remaining one layer of hydration shell.^{43,73} On the other hand, in their dried state, the protein molecules seem to be homogeneously distributed through partial orientation, deformation or interpenetration of the molecules. Studies have also shown that for dry proteins or low water fraction, the plasticization by water is stronger, making the molecule swell.¹⁷ Therefore, in the dried state, the water molecules could also be homogeneously distributed over the matrix of more exposed protein molecules due to their interpenetration instead of forming a complete shell around each protein molecule.

In order to cross-check the validity of the estimated c_p during evaporation from the SAXS data using the power law relation between ξ and c_p (eqn (6)), we performed c_p measurements as a function of evaporation time under different environmental conditions. We used a balance equipped with a weighing chamber. The BSA film was made on the metal ring as was done for the SAXS measurements and placed on the balance. The mass of the solution was monitored over time. This measurement was performed with the weighing chamber of the balance closed, open (both are under ambient conditions) as well as under N_2 (flow) atmosphere.

The protein concentration during drying is determined as follows. We assume that the weighing measurement started with a mass of m_1 (g) of a BSA solution of concentration c_{p1} and after a certain drying time the mass is measured to be m_2 (g). Then the mass of BSA (in g) in the solution is

$$m_{1\text{BSA}} = \frac{m_1 \times V_s^{\text{H}_2\text{O}}}{\left(\frac{1}{c_{p1}} - V_s + V_s^{\text{H}_2\text{O}}\right)}. \quad (10)$$

Here, $m_1 = m_{1\text{BSA}} + m_{1\text{H}_2\text{O}}$, where $m_{1\text{H}_2\text{O}}$ is the mass of water in m_1 g of solution, and $c_{p1} = \frac{m_{1\text{BSA}}}{(m_{1\text{BSA}} \times V_s) + (m_{1\text{H}_2\text{O}} \times V_s^{\text{H}_2\text{O}})}$,

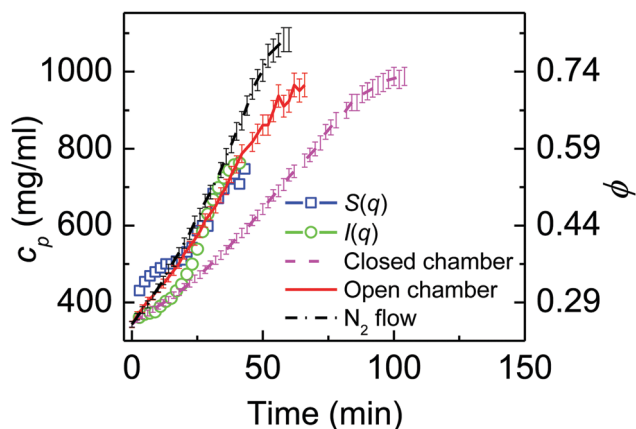


Fig. 4 Comparison of the c_p estimation from $S(q)$ (blue squares), $I(q)$ (green circles), and weighing measurements in the closed cover (magenta dashed line), in the open cover (red solid line) and under N_2 atmosphere (black dashed-dotted line) as a function of evaporation time.

where V_s is the specific volume of BSA ($0.735 \text{ cm}^3 \text{ g}^{-1}$) and $V_s^{\text{H}_2\text{O}}$ is the specific volume of water which is assumed as $1 \text{ (cm}^3 \text{ g}^{-1})$.

Therefore, the new concentration (in g ml^{-1}) is,

$$c_{p2} = \frac{m_{\text{BSA}}}{(m_{\text{BSA}} \times V_s) + (m_{\text{H}_2\text{O}} \times V_s^{\text{H}_2\text{O}})} \quad (11)$$

where, $m_{\text{H}_2\text{O}} = m_2 - m_{\text{BSA}}$.

The evolution of the solution concentration estimated from this measurement is shown in Fig. 4 along with the c_p profile obtained from the SAXS measurements. Interestingly, the c_p profile obtained from SAXS approximately follows a similar evolution of concentration with time (see the data obtained in the open chamber). Although the initial SAXS data points show deviations from those obtained in the open chamber and under N_2 atmosphere, the c_p values approximately match at a later stage. The changes in the shape of the curves (compressed or stretched) are simply due to the difference in the solvent evaporation rates under different atmospheres. These results support the validity of the power law relation used to estimate c_p from the SAXS profiles. Note that dry BSA can reach a ϕ as high as *ca.* 0.74. This value can be even higher if the solution is dried under N_2 atmosphere. Importantly, using our SAXS data, we were able to perform concentration calculations until a c_p range sufficiently high to observe jamming, *i.e.*, when the correlation peak disappears. In addition, Fig. 4 indicates that, although the c_p obtained from $I(q)$ (green circles) and those obtained from the corresponding $S(q)$ (blue squares) are different in the initial stage, they are approximately the same in later stages.

4 Dynamics of the protein solution with increasing ϕ

As a consequence of the structural transition to a jammed state, the microscopic dynamics has been found to slow down enormously in a colloidal or polymeric system.^{74,75} In the present case, to understand the impact of the structural evolution while increasing the volume fraction, we studied the

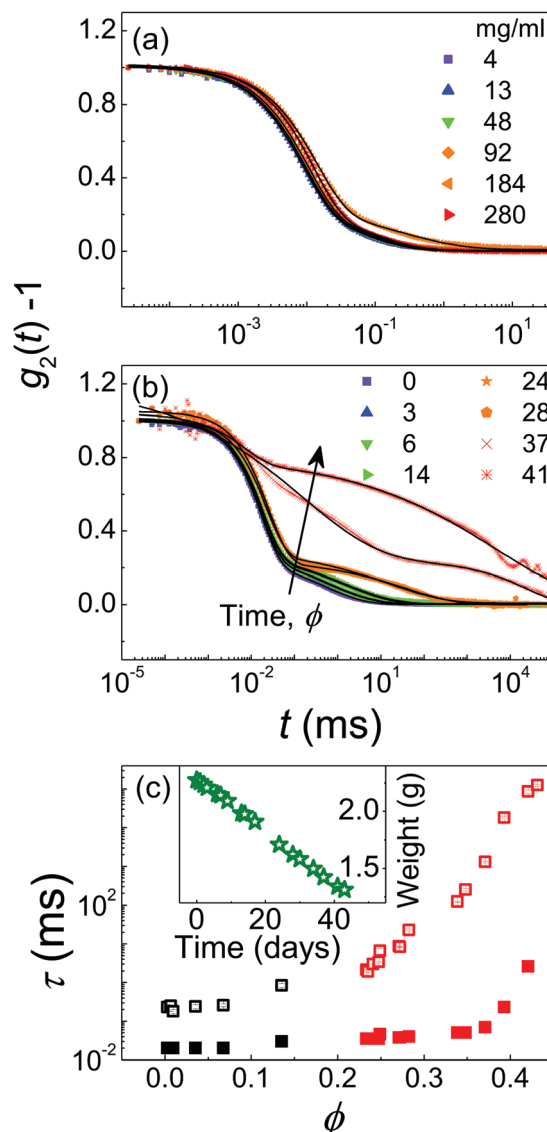


Fig. 5 Representative correlation functions (a) at different concentrations (in mg ml^{-1}) as indicated in the legends (collected on the individual solutions) and (b) at different evaporation times (in days) as indicated in the legends (collected on the drying sample). The arrow indicates the evaporation time (and hence ϕ which increases with time). The solid lines indicate the fits to eqn (3). (c) τ_1 (filled squares) and τ_2 (open squares) as a function of ϕ obtained from DLS measurements on the individual solutions (black symbols) and the drying sample (red symbols) at $q = 0.019 \text{ nm}^{-1}$ (corresponding to $2\theta = 90^\circ$). Error bars are smaller than the symbols. Inset shows the total weight of the solution, during evaporation, as a function of evaporation time (in days).

equilibrium dynamics of the aqueous BSA solution during drying using DLS measurements. $g_2(t)$ functions collected on the individual solutions of different concentrations and those collected on the drying sample are shown in Fig. 5(a and b) at $2\theta = 90^\circ$. The concentration of the drying sample on the first day of measurements is 317 mg ml^{-1} ($\phi = 0.23$) as mentioned previously. A monotonic evolution of the dynamics as the concentration (or ϕ) increases is observed. At low c_p , $g_2(t)$ primarily shows a single decay in the measured time window

of μs to thousands of seconds. As ϕ increases, $g_2(t)$ develops a distinct two-step relaxation decay suggesting a caged motion of the protein molecules.³⁰ Note that the first g_2 collected on the drying sample (*i.e.* at $c_p = 317 \text{ mg ml}^{-1}$) shows a pronounced secondary relaxation decay whereas g_2 obtained from the solution with a c_p of 280 mg ml^{-1} shows a weak secondary relaxation (for better visualization see Fig. S10 in the ESI†). This implies that the secondary mode becomes prominent near or before $c_p = 317 \text{ mg ml}^{-1}$ ($\phi = 0.23$) which could correspond to the first transition from regime (1) to (2) observed (at $\phi = 0.22$) in the SAXS data (see Fig. 3). Such a pronounced secondary relaxation is likely due to the correlated motion of the molecules which have a preferential orientation or are deformed in regime (2).

The change in solution weight due to the evaporation of water during the drying as a function of time is shown in the inset of Fig. 5(c). From this data, using the method described in the ESI,† we estimated the respective c_p as well as ϕ values which are used for further analysis. τ values extracted from the best fit of $g_2(t)$ (black solid lines in Fig. 5(a and b)) are shown in Fig. 5(c). Both fast (τ_1) and slow (τ_2) modes increase with increasing ϕ . Especially the rapid increase of τ_2 , reflecting the α relaxation of the system,³⁰ as a function of ϕ seems to be well described by the Vogel-Fulcher-Tammann (VFT)^{50,51} relation.

Fig. 6(a) shows γ_1 and γ_2 vs. ϕ plots for both decays. The fast component (γ_1) shows an exponential behavior (with $\gamma \approx 1$) suggesting Brownian dynamics.⁵⁶ On the other hand, the slow component (γ_2) shows a stretched exponential behavior ($\gamma_2 \ll 1$) indicating a slow cooperative dynamics.⁷⁷ Such a stretched exponential dynamics, often observed in a glass former,⁷⁸ and the rapid growth of τ_2 with ϕ led us to compare the present dynamics with the VFT relation. We averaged several τ_2 vs. ϕ curves obtained at different q values and fitted with the VFT equation⁷⁹

$$\log(\tau_2) = \log(\tau_0) + \frac{A}{\phi - \phi_c} \quad (12)$$

where ϕ_c is the VFT critical volume fraction, τ_0 is the pre-exponential constant, and A is the fragility parameter. The averaged τ as a function of ϕ along with the average VFT fit are shown in Fig. 6(b). The transition volume fraction obtained from the VFT fit is $\phi_c = 0.49$ corresponding to the jamming which is in good agreement with ref. 45 reporting a kinetic arrest at $\phi = 0.47$. At this stage, the second component of the dynamics (τ_2) becomes extremely high, confirming the presence of a jammed state.

The overall behavior of the system as a function of volume fraction is illustrated schematically in Fig. 7. In regime (1), the molecules are in a solution with a clear correlation peak in $I(q)$ and in $S(q)$. In this case, the dynamics mainly exhibits a single component relaxation decay as shown in the bottom panel of Fig. 7 (regime (1)). In regime (2), the solution consists of molecules oriented or deformed and the peak intensity decreases. The dynamics here shows a pronounced two-step relaxation decay (see bottom panel of Fig. 7 (regime (2))). In regime (3), the molecules form a jammed state due to which the density contrast as well as the correlation peak disappears. In this case, the secondary relaxation becomes extremely slow (see bottom panel of Fig. 7 (regime (3))).

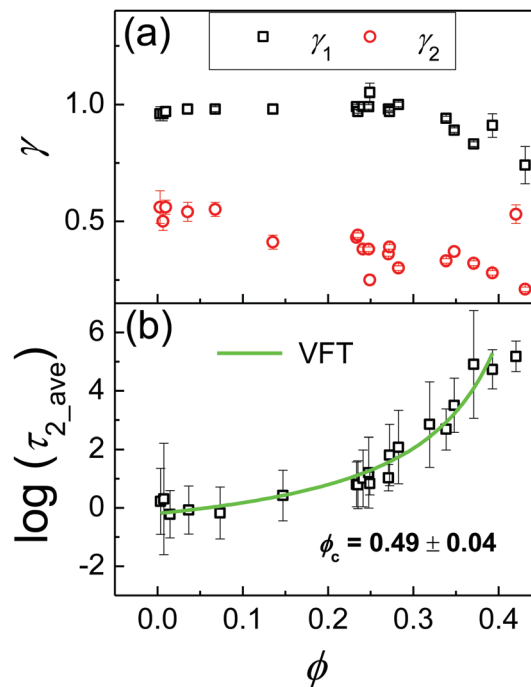


Fig. 6 (a) γ_1 (black squares) and γ_2 (red circles), obtained from the fits in Fig. 5(a and b), as a function of ϕ showing exponential and stretched exponential relaxation dynamics, respectively. (b) τ_2 averaged over different q values as a function of ϕ , along with the VFT fit exhibiting the VFT critical volume fraction of 0.49.

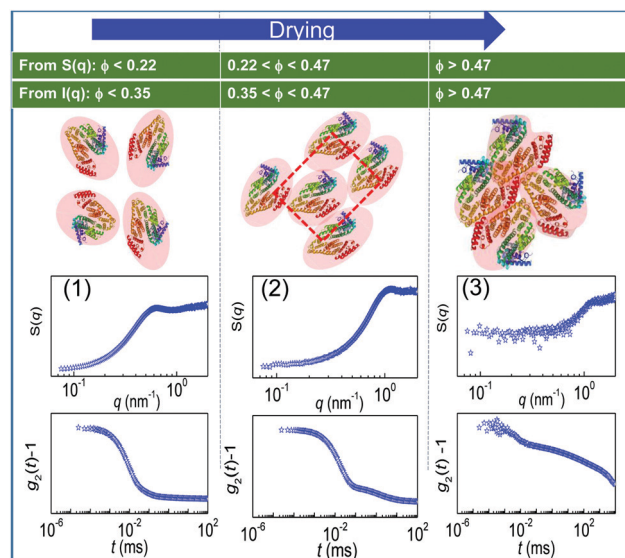


Fig. 7 Schematic illustration of protein molecules in three different regimes; regime (1): dilute state with $\xi > \sigma$, regime (2): $\xi < \sigma$ and regime (3): jammed state (protein structure taken from PDB 3V03⁷⁶).

5 Conclusions

In conclusion, we have studied the packing and the dynamics of the globular protein bovine serum albumin in solution as a function of concentration (c_p) or volume fraction (ϕ) *via* solvent evaporation. We probed the evolution of the inter-protein

distance, ξ , obtained from small angle X-ray scattering experiments. We observed ξ to follow a power law as a function of c_p , initially with an exponent of 0.33 which corresponds to literature values and, at a later stage, with an exponent of 0.41 showing a deviation from the usual behavior at $c_p \sim 200 \text{ mg ml}^{-1}$ ($\phi = 0.15$). We further observed three different regimes of the evolution of ξ with increasing ϕ . Starting from a regime (1) ($\phi < 0.22$), where the intermolecular distance is larger than the size of an individual protein molecule and the dynamics primarily shows a single relaxation decay suggesting Brownian motion, the solution reaches an intermediate regime with molecular orientation and deformation where $0.22 < \phi < 0.47$. In this regime the inter-protein distance becomes smaller than the native protein diameter and the dynamics exhibits a clear two-step relaxation decay. In the third regime, beyond $\phi \sim 0.47$, the SAXS correlation peak slowly disappears. In this regime, the growth of ϕ slows down and eventually becomes stationary at $\phi \sim 0.55$. The secondary relaxation time reaches an extremely high value which is interpreted as the jammed state of the solution with approximately one hydration layer around each protein molecule. This study establishes a connection between the evolution of structural packing and microscopic dynamics with increasing volume fraction in an aqueous globular protein solution.

Conflicts of interest

There are no conflicts of interest to declare.

Acknowledgements

The authors would like to thank the European Synchrotron Radiation Facility (ESRF), Grenoble, France for beamtime allocation on beamline ID02. Deutsche Forschungsgemeinschaft (DFG) has supported this project financially. O. M. acknowledges the Studienstiftung des Deutschen Volkes for a PhD fellowship and N. B. acknowledges the Alexander von Humboldt-Stiftung for a postdoctoral fellowship. The authors also thank Aparna Viswanathan Ammanath for her assistance with the DLS measurements.

Notes and references

- 1 F. Franks, *Biotechnol. Genet. Eng. Rev.*, 1999, **16**, 281–292.
- 2 W. Wang, *Int. J. Pharm.*, 2000, **203**, 1–60.
- 3 D. Asai, D. Xu, W. Liu, F. G. Quiroz, D. J. Callahan, M. R. Zalutsky, S. L. Craig and A. Chilkoti, *Biomaterials*, 2012, **33**, 5451–5458.
- 4 J. H. Crowe, J. F. Carpenter and L. M. Crowe, *Annu. Rev. Physiol.*, 1998, **60**, 73–103.
- 5 J. H. Crowe, L. M. Crowe and D. Chapman, *Science*, 1984, **223**, 701–703.
- 6 R. Y. Yada, *Proteins in food processing*, Woodhead Publishing, 2017.
- 7 T. Sumi and H. Sekino, *Phys. Chem. Chem. Phys.*, 2011, **13**, 15829–15832.
- 8 A. P. Minton, *Biophys. J.*, 2005, **88**, 971–985.
- 9 C. M. Miller, Y. C. Kim and J. Mittal, *Biophys. J.*, 2016, **111**, 28–37.
- 10 A. Bhattacharya, Y. C. Kim and J. Mittal, *Biophys. Rev.*, 2013, **5**, 99–108.
- 11 J. Hansen, F. Platten, D. Wagner and S. U. Egelhaaf, *Phys. Chem. Chem. Phys.*, 2016, **18**, 10270–10280.
- 12 D. Homouz, M. Perham, A. Samiotakis, M. S. Cheung and P. Wittung-Stafshede, *Proc. Natl. Acad. Sci. U. S. A.*, 2008, **105**, 11754–11759.
- 13 M. Delarue, G. Brittingham, S. Pfeffer, I. Surovtsev, S. Pinglay, K. Kennedy, M. Schaffer, J. Gutierrez, D. Sang and G. Poterewicz, *et al.*, *Cell*, 2018, **174**, 338–349.
- 14 S. Smith, C. Cianci and R. Grima, *J. R. Soc., Interface*, 2017, **14**, 20170047.
- 15 H.-X. Zhou, G. Rivas and A. P. Minton, *Annu. Rev. Biophys.*, 2008, **37**, 375–397.
- 16 D. Laage, T. Elsaesser and J. T. Hynes, *Chem. Rev.*, 2017, **117**, 10694–10725.
- 17 A. Panagopoulou, A. Kyritsis, N. Shinyashiki and P. Pissis, *J. Phys. Chem. B*, 2012, **116**, 4593–4602.
- 18 T. Ando and J. Skolnick, *Proc. Natl. Acad. Sci. U. S. A.*, 2010, **107**, 18457–18462.
- 19 M. Yu, T. C. Silva, A. van Opstal, S. Romeijn, H. A. Every, W. Jiskoot, G.-J. Witkamp and M. Ottens, *Biophys. J.*, 2019, **116**, 595–609.
- 20 F. Roosen-Runge, M. Hennig, T. Seydel, F. Zhang, M. W. Skoda, S. Zorn, R. M. Jacobs, M. Maccarini, P. Fouquet and F. Schreiber, *Biochim. Biophys. Acta, Proteins Proteomics*, 2010, **1804**, 68–75.
- 21 F. Roosen-Runge, M. Hennig, F. Zhang, R. M. Jacobs, M. Sztucki, H. Schober, T. Seydel and F. Schreiber, *Proc. Natl. Acad. Sci. U. S. A.*, 2011, **108**, 11815–11820.
- 22 A. Giannopoulou, A. Aletras, N. Pharmakakis, G. Papatheodorou and S. Yannopoulos, *J. Chem. Phys.*, 2007, **127**, 11B617.
- 23 S. Bucciarelli, J. S. Myung, B. Farago, S. Das, G. A. Vliegthart, O. Holderer, R. G. Winkler, P. Schurtenberger, G. Gompper and A. Stradner, *Sci. Adv.*, 2016, **2**, e1601432.
- 24 M. M. Castellanos, N. J. Clark, M. C. Watson, S. Krueger, A. McAuley and J. E. Curtis, *J. Phys. Chem. B*, 2016, **120**, 12511–12518.
- 25 A. Stradner, H. Sedgwick, F. Cardinaux, W. C. Poon, S. U. Egelhaaf and P. Schurtenberger, *Nature*, 2004, **432**, 492.
- 26 T. Sumi, H. Imamura, T. Morita and K. Nishikawa, *J. Mol. Liq.*, 2014, **200**, 42–46.
- 27 R. Akiyama, T. Yamashita and S. Fujihara, *J. Mol. Liq.*, 2014, **200**, 72–76.
- 28 S. Torquato and F. H. Stillinger, *J. Phys. Chem. B*, 2001, **105**, 11849–11853.
- 29 M. D. Rintoul and S. Torquato, *Phys. Rev. E: Stat. Phys., Plasmas, Fluids, Relat. Interdiscip. Top.*, 1998, **58**, 532.
- 30 G. Brambilla, D. El Masri, M. Pierno, L. Berthier, L. Cipelletti, G. Petekidis and A. B. Schofield, *Phys. Rev. Lett.*, 2009, **102**, 085703.
- 31 A. Yethiraj and A. van Blaaderen, *Nature*, 2003, **421**, 513.
- 32 W. Gotze and L. Sjogren, *Rep. Prog. Phys.*, 1992, **55**, 241.

- 33 P. N. Segre, V. Prasad, A. B. Schofield and D. Weitz, *Phys. Rev. Lett.*, 2001, **86**, 6042.
- 34 Z. Wang, H. Guo, Y. Liu and X. Wang, *J. Chem. Phys.*, 2018, **149**, 084905.
- 35 G. A. Vliegthart, A. van Blaaderen and H. N. W. Lekkerkerker, *Faraday Discuss.*, 1999, **112**, 173–181.
- 36 A. Stradner and P. Schurtenberger, *Soft Matter*, 2020, **16**, 307–323.
- 37 M. van Hecke, *J. Phys.: Condens. Matter*, 2009, **22**, 033101.
- 38 K. N. Nordstrom, E. Verneuil, P. Arratia, A. Basu, Z. Zhang, A. G. Yodh, J. P. Gollub and D. J. Durian, *Phys. Rev. Lett.*, 2010, **105**, 175701.
- 39 A. Ikeda, L. Berthier and P. Sollich, *Soft Matter*, 2013, **9**, 7669–7683.
- 40 M. Braibanti, H. S. Kim, N. Senbil, M. J. Pagenkopp, T. G. Mason and F. Scheffold, *Sci. Rep.*, 2017, **7**, 13879.
- 41 P. Hebbeker, F. A. Plamper and S. Schneider, *Macromol. Theory Simul.*, 2018, **27**, 1800033.
- 42 E. Zaccarelli and W. C. Poon, *Proc. Natl. Acad. Sci. U. S. A.*, 2009, **106**, 15203–15208.
- 43 F. Zhang, F. Roosen-Runge, M. W. Skoda, R. M. Jacobs, M. Wolf, P. Callow, H. Frielinghaus, V. Pipich, S. Prevost and F. Schreiber, *Phys. Chem. Chem. Phys.*, 2012, **14**, 2483–2493.
- 44 F. L. González Flecha and V. Levi, *Biochem. Mol. Biol. Educ.*, 2003, **31**, 319–322.
- 45 G. J. Brownsey, T. R. Noel, R. Parker and S. G. Ring, *Biophys. J.*, 2003, **85**, 3943–3950.
- 46 L. R. Barbosa, M. G. Ortore, F. Spinozzi, P. Mariani, S. Bernstorff and R. Itri, *Biophys. J.*, 2010, **98**, 147–157.
- 47 C. C. Michel, M. E. Phillips and M. R. Turner, *J. Physiol.*, 1985, **360**, 333–346.
- 48 P. Caironi and L. Gattinoni, *Blood Transfus.*, 2009, **7**, 259.
- 49 R. B. Reeves, *J. Appl. Physiol.*, 1976, **40**, 762–767.
- 50 W.-S. Xu, J. F. Douglas and K. F. Freed, *Macromolecules*, 2017, **50**, 2585–2598.
- 51 Z. Evenson, B. Ruta, S. Hechler, M. Stolpe, E. Pineda, I. Gallino and R. Busch, *Phys. Rev. Lett.*, 2015, **115**, 175701.
- 52 S. Da Vela, M. K. Braun, A. Dörr, A. Greco, J. Möller, Z. Fu, F. Zhang and F. Schreiber, *Soft Matter*, 2016, **12**, 9334–9341.
- 53 H. A. Sober, *CRC Handbook of Biochemistry: Selected data for molecular biology*, The Chemical Rubber Co., Cleveland, Ohio, 1970.
- 54 Y. Li, V. Lubchenko and P. G. Vekilov, *Rev. Sci. Instrum.*, 2011, **82**, 053106.
- 55 B. J. Berne and R. Pecora, *Dynamic light scattering: with applications to chemistry, biology, and physics*, Courier Corporation, 2000.
- 56 S. K. Sinha, Z. Jiang and L. B. Lurio, *Adv. Mater.*, 2014, **26**, 7764–7785.
- 57 H. Conrad, F. Lehmkuehler, B. Fischer, F. Westermeier, M. Schroer, Y. Chushkin, C. Gutt, M. Sprung and G. Gruebel, *Phys. Rev. E: Stat., Nonlinear, Soft Matter Phys.*, 2015, **91**, 042309.
- 58 T. Narayanan, M. Sztucki, P. Van Vaerenbergh, J. Léonardon, J. Gorini, L. Claustre, F. Sever, J. Morse and P. Boesecke, *J. Appl. Crystallogr.*, 2018, **51**, 1511–1524.
- 59 S. H. Klapp, D. Qu and R. V. Klitzing, *J. Phys. Chem. B*, 2007, **111**, 1296–1303.
- 60 C. V. Raman, *Philos. Mag.*, 1924, **47**, 671–679.
- 61 S. Hansen, *J. Appl. Crystallogr.*, 2013, **46**, 1008–1016.
- 62 G. M. Conley, P. Aebischer, S. Nöjd, P. Schurtenberger and F. Scheffold, *Sci. Adv.*, 2017, **3**, e1700969.
- 63 A. Donev, I. Cisse, D. Sachs, E. A. Variano, F. H. Stillinger, R. Connelly, S. Torquato and P. M. Chaikin, *Science*, 2004, **303**, 990–993.
- 64 M. A. Klatt and S. Torquato, *Phys. Rev. E*, 2016, **94**, 022152.
- 65 T. Arakawa and S. N. Timasheff, *Biochemistry*, 1982, **21**, 6536–6544.
- 66 T. V. Chalikian, M. Totrov, R. Abagyan and K. J. Breslauer, *J. Mol. Biol.*, 1996, **260**, 588–603.
- 67 P. S. Mohanty, S. Nöjd, K. van Gruijthuijsen, J. J. Crassous, M. Obiols-Rabasa, R. Schweins, A. Stradner and P. Schurtenberger, *Sci. Rep.*, 2017, **7**, 1487.
- 68 B. Crist, *J. Polym. Sci., Part B: Polym. Phys.*, 2001, **39**, 2454–2460.
- 69 J. Liu, H.-J. Schöpe and T. Palberg, *Part. Part. Syst. Charact.*, 2000, **17**, 206–212.
- 70 M. L. de Haro and M. Robles, *J. Phys.: Condens. Matter*, 2004, **16**, S2089.
- 71 M. Mailman, C. F. Schreck, C. S. O. Hern and B. Chakraborty, *Phys. Rev. Lett.*, 2009, **102**, 255501.
- 72 A. Boromand, A. Signoriello, F. Ye, C. S. O'Hern and M. D. Shattuck, *Phys. Rev. Lett.*, 2018, **121**, 248003.
- 73 D. Svergun, S. Richard, M. Koch, Z. Sayers, S. Kuprin and G. Zaccai, *Proc. Natl. Acad. Sci. U. S. A.*, 1998, **95**, 2267–2272.
- 74 M. Bellour, A. Knaebel, J. Harden, F. Lequeux and J.-P. Munch, *Phys. Rev. E: Stat., Nonlinear, Soft Matter Phys.*, 2003, **67**, 031405.
- 75 R. Bandyopadhyay, D. Liang, H. Yardimci, D. A. Sessoms, M. A. Borthwick, S. Mochrie, J. L. Harden and R. L. Leheny, *Phys. Rev. Lett.*, 2004, **93**, 228302.
- 76 K. A. Majorek, P. J. Porebski, A. Dayal, M. D. Zimmerman, K. Jablonska, A. J. Stewart, M. Chruszcz and W. Minor, *Mol. Immunol.*, 2012, **52**, 174–182.
- 77 S. Manley, H. Wyss, K. Miyazaki, J. Conrad, V. Trappe, L. Kaufman, D. Reichman and D. Weitz, *Phys. Rev. Lett.*, 2005, **95**, 238302.
- 78 S. Jabbari-Farouji, G. H. Wegdam and D. Bonn, *Phys. Rev. Lett.*, 2007, **99**, 065701.
- 79 A.-M. Philippe, D. Truzzolillo, J. Galvan-Myoshi, P. Dieudonné-George, V. Trappe, L. Berthier and L. Cipelletti, *Phys. Rev. E*, 2018, **97**, 040601.